DØ Note 6183-CONF

Combined Upper Limits on Standard Model Higgs Boson Production in the W^+W^-, $\tau\tau$ and $\gamma\gamma$ decay modes in up to 8.2 fb^{-1} of data from the DØ Experiment

The DØ Collaboration
URL http://www-d0.fnal.gov
(Dated: March 14, 2011)

Searches for standard model Higgs boson production in $p\bar{p}$ collisions at $\sqrt{s} = 1.96$ TeV are carried out for Higgs boson masses (M_H) in the range $130 \leq M_H \leq 200$ GeV. The results presented here focus on the dominant decay mode in this mass range, namely Higgs boson decays into W^+W^-, although contributions from decays into $\tau^+\tau^-$ and $\gamma\gamma$ are also included. The contributing production processes include gluon-gluon fusion ($gg \rightarrow H$), associated production ($q\bar{q} \rightarrow W/ZH$) and vector boson fusion ($q\bar{q} \rightarrow q\bar{q}H$). Analyses are conducted with integrated luminosities ranging from 4.3 to 8.2 fb^{-1}. As no significant excess is observed, we set limits on standard model Higgs boson production. The observed 95% C.L. upper limits are found to be a factor of 0.75 times the predicted standard model cross section at M_H =165 GeV while the expected limit is found to be a factor of 0.92 times the standard model prediction for the same mass. We exclude at the 95% C.L. the region $163 < M_H < 168$ GeV with an a-priori expected exclusion of $160 < M_H < 168$ GeV.

I. INTRODUCTION

Despite its success as a predictive tool, the standard model (SM) of particle physics remains incomplete without a means to explain electroweak symmetry breaking. The simplest proposed mechanism involves the introduction of a complex doublet of scalar fields that generate the masses of elementary particles via their mutual interactions. After accounting for longitudinal polarizations for the electroweak bosons, this so-called Higgs mechanism also gives rise to a single scalar boson with an unpredicted mass. Direct searches in $e^+e^- \to Z^* \to ZH$ at the Large Electron Positron (LEP) collider yielded a lower mass limit at $M_H > 114.4$ GeV [1] while precision electroweak data yield the indirect constraint $M_H < 158$ GeV [2], with both limits set at 95% confidence level (C.L.). When also considering the direct limit, the indirect constraint predicts $M_H < 185$ GeV, indicating that the range $100 \leq M_H \leq 200$ GeV is the most important search region for a SM Higgs boson. The search for a SM Higgs boson is one of the main goals of the Fermilab Tevatron physics program.

In this note, we combine the results of direct searches for SM Higgs bosons in $p\bar{p}$ collisions at $\sqrt{s} = 1.96$ TeV recorded by the DØ experiment [3]. The analyses combined here seek signals of Higgs bosons produced through gluon-gluon fusion (GGF) ($gg \to H$), in association with vector bosons ($q\bar{q} \to VH$ where $V = W, Z$) and through vector boson fusion (VBF) ($q\bar{q} \to q'\bar{q}'H$). The analyses utilize data corresponding to integrated luminosities ranging from 4.3 to 8.2 fb^{-1}, collected during the period 2002-2010. The Higgs boson decay modes studied are $H \to W^+W^-$, $H \to \tau^+\tau^-$ and $H \to \gamma\gamma$. The searches are organized into 34 analysis subsets comprising different production, decay and final state particle configurations, each designed to isolate a particular Higgs boson production and decay mode. In order to facilitate proper combination of signals, the analyses were designed to be mutually exclusive after analysis selections. Searches for several final states are performed in two distinct epochs of data collection: before and after the 2006 DØ detector upgrade. The largest changes made during the upgrade were the addition of a new layer to the silicon detector nearest to the beam-line and an upgrade of the trigger system. The two epochs are denoted as Run IIa (1.1 fb^{-1}) and Run IIb (on-going, currently up to 7.1 fb^{-1}are analyzed in this note).

The analyses used in this combination [4–9] are outlined in Table I. The dominant search mode in the mass range considered involves a Higgs boson decaying into two $W^\pm$ bosons, and the three dominant production mechanisms: gluon-gluon fusion, associated production and vector-boson fusion. In the case of production via gluon-gluon fusion and vector-boson fusion, we search for leptonic W boson decays with five final states of opposite-signed leptons: $WW \to e^+\nu e^-\nu$, $e^\pm\nu\mu^\mp\nu$, $\mu^+\nu\mu^-\nu$, $e^\pm\nu\tau^\mp_{had}\nu$ and $\mu^\pm\nu\tau^\mp_{had}\nu$, where τ_{had} denotes a hadronic tau decay. In addition we consider final states originating from Higgs boson production in association with a vector boson (WH or ZH), where leptons may originate from the vector boson or Higgs boson decay. We classify events according to their jet multiplicity in order to isolate particular signal production mechanisms and optimize the signal-to-background discrimination. The $H \to W^+W^- \to \ell^\pm\nu\ell^\mp\nu$ ($l = e, \mu$) analyses further separate events in three final states with 0 jets, 1 jet, and 2 or more jets. Analyses identifying hadronic tau candidates select events with ≤ 1 jets, mainly sensitive to the gluon-gluon fusion signal, or with ≥ 2 jets, also sensitive to associated production and vector-boson fusion. At high mass, the dominant signal contribution to both tau analyses originates from $H \to W^+W^- \to \mu^\pm\nu\tau^\mp\nu$.

A separate analysis considers the semileptonic decay $H \to W^+W^- \to \ell\nu q\bar{q}$. In all $H \to W^+W^-$ decays with $M_H < 2M_W$, at least one of the W bosons will be off mass shell. For $VH \to \ell^\pm\ell^\pm + X$ production, we search for leptonic W boson decays with three final states of same-signed leptons: $VWW \to e^\pm\nu e^\pm\nu + X$, $e^\pm\nu\mu^\pm\nu + X$, and $\mu^\pm\nu\mu^\pm\nu + X$. Finally, we include an analysis that searches for Higgs bosons decaying to two photons and produced via gluon-gluon fusion, vector boson fusion, and associated production mechanisms.

Since the most recent DØ SM combined Higgs boson search results [10], we have updated the $H \to W^+W^- \to \ell^\pm\nu\ell^\mp\nu$, $H \to W^+W^- \to \ell\nu q\bar{q}$, $H + X \to \ell^\pm\tau^\mp_{had}jj$ and $H \to \gamma\gamma$ analyses. The $H + X \to \mu^\pm\tau^\mp_{had} + \leq 1j$ channel is a new addition to the combination. In some cases, particular analyses or sub-channels of an analysis were not updated and the previous results were used: the $VH \to \ell^\pm\ell^\pm + X$analysis and the Run IIa channels of the $H \to W^+W^- \to e^\pm\nu\mu^\mp\nu$ analyses.

The backgrounds from multijet production are measured in data. The other backgrounds were generated by PYTHIA [11], ALPGEN [12], and COMPHEP [13], with PYTHIA providing parton-showering and hadronization. Background cross sections are normalized either to next-to-leading order (NLO) calculations from MCFM [14] or, whenever possible, to data control samples.

II. SIGNAL PREDICTIONS AND UNCERTAINTIES

A common approach to the signal predictions and associated uncertainties is followed by the CDF and DØ Collaborations. An outline of the procedures followed is given here, more complete discussion can be found in Ref. [15]. We normalize our Higgs boson signal predictions to the most recent highest-order calculations available, for all production processes considered. The largest production cross section, $\sigma(gg \to H)$, is calculated at next-to-next-to-leading order (NNLO) in QCD with soft gluon resummation to next-to-next-to-leading-log (NNLL) accuracy, and also includes

TABLE I: List of analysis channels, corresponding integrated luminosities, and final variables used for setting limits, which in most cases is a decision-tree (DTree) or neural-network (NN) discriminant. See Sect. I for details ($\ell = e, \mu$).

Channel	Luminosity (fb^{-1})	Final Variable	# Sub-Channels	Reference
$H\to W^+W^-\to\ell^\pm\nu\ell^\mp\nu$, 0/1/2+ jet	8.1	DTree discriminant	18	[4]
$H\to W^+W^-\to\ell\nu q\bar{q}$	5.4	DTree discriminant	4	[5]
$H+X\to\mu^\pm\tau^\mp_{had}+\leq 1j$	7.3	NN	3	[6]
$H+X\to\mu^\pm\tau^\mp_{had}jj$	4.3	DTree discriminant	2	[7]
$H+X\to e^\pm\tau^\mp_{had}jj$	4.3	DTree discriminant	1	[7]
$VH\to\ell^\pm\ell^\pm+X$	5.3	DTree discriminant	6	[8]
$H\to\gamma\gamma$	8.2	DTree discriminant	1	[9]

two-loop electroweak effects and handling of the running b quark mass [16, 17]. The numerical values in Table II are updates [18] of these predictions with m_t set to 173.1 GeV/c^2 [19], and an exact treatment of the massive top and bottom loop corrections up to NLO+NLL. The factorization and renormalization scale choice for this calculation is $\mu_F = \mu_R = M_H$. These calculations are refinements of the earlier NNLO calculations of the $gg \to H$ production cross section [20–22]. Electroweak corrections were computed in Refs. [23, 24]. Soft gluon resummation was introduced in the prediction of the $gg \to H$ production cross section in Ref. [25].

The $gg \to H$ production cross section depends strongly on the gluon parton density function, and the accompanying value of $\alpha_s(q^2)$. The cross sections used here are calculated with the MSTW08 NNLO PDF set [26], as recommended by the PDF4LHC working group [27], as this PDF parameterization is the only NNLO prescription that results from a fully global fit. We follow the PDF4LHC working group's prescription to evaluate the uncertainties on the $gg \to H$ production cross section due to the PDFs. This prescription is to evaluate the predictions of $\sigma(gg \to H)$ at NLO using the global NLO PDF sets CTEQ6.6 [28], MSTW08 [26], and NNPDF2.0 [29], and to take the envelope of the predictions and their uncertainties due to PDF+α_s for the three sets as the uncertainty range at NLO. The ratio of the NLO uncertainty range to that of just MSTW08 is then used to scale the NNLO MSTW08 PDF+α_s uncertainty, to estimate a larger uncertainty at NNLO. This procedure roughly doubles the PDF+α_s uncertainty from MSTW08 at NNLO alone. Additional discussion of why we believe this choice of PDF set and error calculation is appropriate is given in Ref. [15].

We also include uncertainties on $\sigma(gg \to H)$ due to uncalculated higher order processes by following the standard procedure of varying the factorization renormalization scales up and down together by a factor $\kappa = 2$, as this produces the maximum impact on $\sigma(gg \to H)$. At a central scale choice of $\mu_R = \mu_F = M_H/2$, the fixed-order calculations at NLO and NNLO converge rapidly and the scale uncertainties generously cover the differences. Furthermore, the NNLO calculation using a scale choice of $\mu_R = \mu_F = M_H/2$ is very close to the NNLL+NNLO calculation that we use. The authors of the NNLL+NNLO calculation recommend that we use the scale choice $\mu_R = \mu_F = M_H$ for the central value [17]. The uncertainty on $\sigma(gg \to H)$ is evaluated by varying $\mu_R = \mu_F$ from a lower value of $M_H/2$ to an upper value of $2M_H$, the customary variation, and by evaluating the NNLO+NNLL cross sections at these scales.

Because the $H \to W^+W^-$ analyses separate the data into categories based on the numbers of observed jets, we assess factorization and renormalization scale and PDF+α_s variations separately for each jet category as evaluated in Ref. [30]. This calculation is at NNLO for H+0 jets, at NLO for H+1 jet, and at LO for H+2 or more jets. A newer, more precise calculation [31] of the H+2 or more jets cross section at NLO is used to evaluate the uncertainties in this category. These scale uncertainties are used instead of the inclusive NNLL+NNLO scale uncertainty because we require them in each jet category, and the uncertainties we use are significantly larger than the inclusive scale uncertainty. The scale choice affects the p_T spectrum of the Higgs boson when produced in gluon-gluon fusion, and this effect changes the acceptance of the selection requirements and also the shapes of the distributions of the final discriminants. The effect of the acceptance change is included in the calculations of Ref. [30] and Ref. [31], as the experimental requirements are simulated in these calculations. The effects on the final discriminant shapes are obtained by reweighting the p_T spectrum of the Higgs boson production in our Monte Carlo simulation to higher-order calculations. The Monte Carlo signal simulation is provided by the LO generator PYTHIA (with CTEQ5L and CTEQ6L [32] leading-order (LO) parton distribution functions) which includes a parton shower and fragmentation and hadronization models. We reweight the Higgs boson p_T spectra in our PYTHIA Monte Carlo samples to that predicted by HQT [33] when making predictions of differential distributions of $gg \to H$ signal events. To evaluate the impact of the scale uncertainty on our differential spectra, we use the RESBOS [34] generator, and apply the scale-dependent differences in the Higgs boson p_T spectrum to the HQT prediction, and propagate these to our final discriminants as a systematic uncertainty on the shape, which is included in the calculation of the limits.

We treat the scale uncertainties as 100% correlated between jet categories, the PDF+α_s uncertainties in the cross

TABLE II: The production cross sections (in fb) and decay branching fractions (in %) for the SM Higgs boson assumed for the combination.

m_H (GeV/c^2)	$\sigma_{gg\to H}$	σ_{WH}	σ_{ZH}	σ_{VBF}	$B(H\to\tau^+\tau^-)$	$B(H\to W^+W^-)$	$B(H\to ZZ)$	$B(H\to\gamma\gamma)$
130	842.9	112.00	68.5	62.1	5.305	29.43	3.858	0.2182
135	750.8	97.20	60.0	57.5	4.400	39.10	5.319	0.2077
140	670.6	84.60	52.7	53.2	3.472	49.16	6.715	0.1897
145	600.6	73.70	46.3	49.4	2.585	59.15	7.771	0.1653
150	539.1	64.40	40.8	45.8	1.778	68.91	8.143	0.1357
155	484.0	56.20	35.9	42.4	1.057	78.92	7.297	0.1000
160	432.3	48.50	31.4	39.4	0.403	90.48	4.185	0.0537
165	383.7	43.60	28.4	36.6	0.140	95.91	2.216	0.0233
170	344.0	38.50	25.3	34.0	0.093	96.39	2.351	0.0160
175	309.7	34.00	22.5	31.6	0.073	95.81	3.204	0.0124
180	279.2	30.10	20.0	29.4	0.059	93.25	5.937	0.0102
185	252.1	26.90	17.9	27.3	0.046	84.50	14.86	0.0081
190	228.0	24.00	16.1	25.4	0.038	78.70	20.77	0.0068
195	207.2	21.40	14.4	23.7	0.033	75.88	23.66	0.0059
200	189.1	19.10	13.0	22.0	0.029	74.26	25.33	0.0053

section are treated likewise. The PDF+α_s uncertainty is however treated as uncorrelated with the scale uncertainty, primarily as the PDF uncertainty arises from experimental uncertainties and PDF parameterization choices, while the scale uncertainty arises from neglected higher-order terms in the perturbative cross section calculations. The PDF predictions do depend on the scale choice, however, and the impact of this on $\sigma(gg\to H)$ is included as part of the scale uncertainty and not as part of the PDF uncertainty, to ensure that all scale dependence is considered correlated. Furthermore, we have verified [35] that the fractional change in the prediction of $\sigma(gg\to H)$ due to the PDF variation depends negligibly on the numerical value of the scale choice, justifying the treatment of PDF and scale uncertainties as uncorrelated. Systematic uncertainties arising from uncorrelated sources are considered to fluctuate independently of one another.

Another source of uncertainty in the prediction of $\sigma(gg\to H)$ is the extrapolation of the QCD corrections computed for the heavy top quark loops to the light-quark loops included as part of the electroweak corrections. Uncertainties at the level of 1-2% are already included in the cross section values we use [16, 17]. In Ref. [16], it is argued that the factorization of QCD corrections is known to work well for Higgs boson masses many times in excess of the masses of the loop particles. A 4% change in the predicted cross section is seen when all QCD corrections are removed from the diagrams containing light-flavored quark loops, which is too conservative. For the b quark loop, which is computed separately in Ref. [16], the QCD corrections are much smaller than for the top loop, further giving confidence that it does not introduce large uncertainties.

We include all significant Higgs production modes in our searches. Besides gluon-gluon fusion (GGF) through virtual quark loops, we include Higgs boson production in association with a W or Z vector boson, and vector boson fusion (VBF). We use the WH and ZH production cross sections computed at NNLO in Ref. [36]. This calculation starts with the NLO calculation of V2HV [37] and includes NNLO QCD contributions [38], as well as one-loop electroweak corrections [39]. We use the VBF cross section computed at NNLO in QCD in Ref. [40]. Electroweak corrections to the VBF production cross section are computed with the HAWK program [41], and are very small (0.03 fb and less) for the Higgs boson mass range considered here.

The Higgs boson decay branching ratio predictions are calculated with HDECAY [42], and are also listed in Table II. We use HDECAY Version 3.53. While the HWW coupling is well predicted, $B(H\to W^+W^-)$ depends on the partial widths of all other Higgs boson decays. The partial width $\Gamma(H\to b\bar{b})$ is sensitive to m_b and α_s, $\Gamma(H\to c\bar{c})$ is sensitive to m_c and α_s, and $\Gamma(H\to gg)$ is sensitive to α_s. The impacts of these uncertainties on $B(H\to W^+W^-)$ depend on M_H due to the fact that $B(H\to b\bar{b})$, $B(H\to c\bar{c})$, $B(H\to gg)$ become very small for Higgs boson masses above 160 GeV/c^2, while they have a larger impact for lower M_H. We use the uncertainties on the branching fraction $B(H\to W^+W^-)$ from Ref. [43]. At $M_H = 130$ GeV/c^2, for example, the m_b variation gives a $^{-4.89}_{+1.70}$% relative variation in $B(H\to W^+W^-)$, α_s gives a $^{-1.02}_{+1.09}$% variation, and m_c gives a $^{-0.45}_{+0.51}$% variation. At $M_H = 165$ GeV/c^2, all three of these uncertainties drop below 0.1%.

III. LIMIT CALCULATIONS

We combine results using the CL_s method with a negative log-likelihood ratio (LLR) test statistic [44]. The value of CL_s is defined as $CL_s = CL_{s+b}/CL_b$ where CL_{s+b} and CL_b are the confidence levels for the signal-plus-background hypothesis and the background-only hypothesis, respectively. These confidence levels are evaluated by integrating corresponding LLR distributions populated by simulating outcomes via Poisson statistics. Separate channels and bins are combined by summing LLR values over all bins and channels. This method provides a robust means of combining individual channels while maintaining individual channel sensitivities and incorporating systematic uncertainties. Systematics are treated as Gaussian uncertainties on the expected number of signal and background events, not the outcomes of the limit calculations. This approach ensures that the uncertainties and their correlations are propagated to the outcome with their proper weights. The CL_s approach used in this combination utilizes binned final-variable distributions rather than a single-bin (fully integrated) value for each contributing analysis. The exclusion criteria are determined by increasing the signal cross section until $CL_s = 1 - \alpha$, which defines a signal cross section excluded at 95% confidence level for $\alpha = 0.95$.

A. Final Variable Preparation

The final variables for all analyses (See Table I) are shown in Figs. 1-4. In several of these figures, multiple contributing sub-processes of common sources are summed together. All analyses are performed on a fine Higgs boson mass grid (every 5 GeV).

B. Systematic Uncertainties

The systematic uncertainties differ between analyses for both the signals and backgrounds [4–9]. Here we summarize only the largest contributions. Most analyses carry an uncertainty on the integrated luminosity of 6.1 [45], while the overall normalization of other analyses is determined from the NNLO Z/γ^* cross section in data events near the peak of $Z \to \ell\ell$ decays. Analyses involving b-tagging have an uncertainty on the b-tagging rate of $\sim 10\%$. The uncertainty on the jet measurement and acceptance is $\sim 7\%$. All analyses include uncertainties associated with lepton measurement and acceptances, which range from 1-9% depending on the final state. The largest contribution for all analyses is the uncertainty on the background cross sections at 4-30% depending on the analysis channel and specific background. These values include both the uncertainty on the theoretical cross section calculations and the uncertainties on the higher order correction factors. The uncertainty on the expected multijet background is dominated by the statistics of the data sample from which it is estimated, and is considered separately from the other cross section uncertainties. The $H \to \gamma\gamma$ analysis also assigns two 8% uncertainties to the NNLO gluon-glun fusion Higgs production cross section associated with the accuracy of the theoretical calculation and arising from uncertainty both in PDF and scale. As discussed the $H \to W^+W^- \to \ell^\pm\nu\ell'^\mp\nu$ ($\ell, \ell' = e, \mu$) analyses apply a different uncertainties for each jet multiplicity final state, ranging from 7% and 17% respectively in the 0-jet bin to 33% and 30% respectively in the 2-jet bin [30]. In addition, several analyses incorporate shape-dependent uncertainties on the kinematics of the dominant backgrounds in the analyses. These shapes are derived from the potential variations of the final variables due to generator and background modeling uncertainties. Further details on the systematic uncertainties are given in Tables III, IV, VI, V, VII, and VIII.

The systematic uncertainties for background rates are generally several times larger than the signal expectation itself and are an important factor in the calculation of limits. Each systematic uncertainty is folded into the signal and background expectations in the limit calculation via Gaussian distributions. These Gaussian values are sampled for each Poisson MC trial (pseudo-experiment). Several of the systematic uncertainties, for example the jet energy scale uncertainty, typically impact the shape of the final variable. These shape dependences were preserved in the description of systematic fluctuations for each Poisson trial. Correlations between systematic sources are carried through in the calculation. For example, the uncertainty on the integrated luminosity is held to be correlated between all signals and backgrounds and, thus, the same fluctuation in the luminosity is common to all channels for a single pseudo-experiment. All systematic uncertainties originating from a common source are held to be correlated, as detailed in Table IX.

To minimize the degrading effects of systematics on the search sensitivity, the individual background contributions are fitted to the data observation by maximizing a likelihood function for each hypothesis [46]. The likelihood is a joint Poisson probability over the number of bins in the calculation and is a function of the nuisance parameters in the system and their associated uncertainties, which are given an additional Gaussian constraint associated with their prior predictions. The maximization of the likelihood function is performed over the nuisance parameters. A fit is

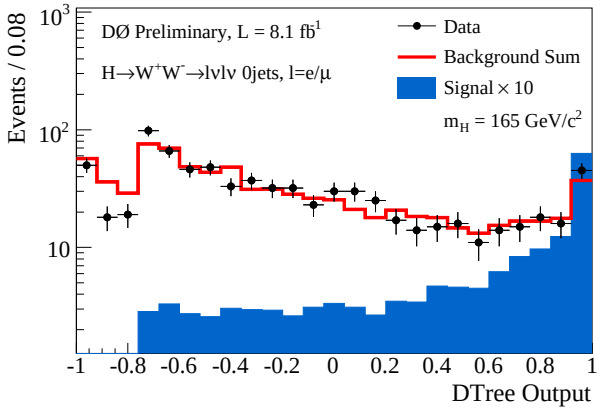

(a) $H \to WW \to ee/\mu\mu$ 0 Jets

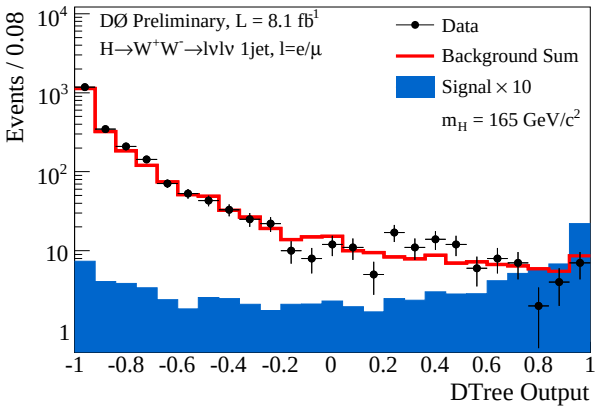

(b) $H \to WW \to ee/\mu\mu$ 1 Jet

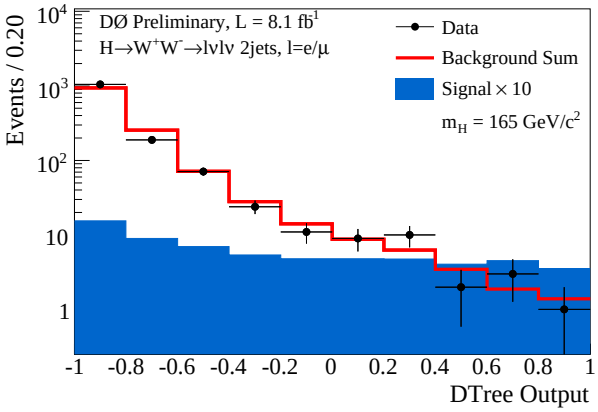

(c) $H \to WW \to ee/\mu\mu$ 2 Jets

FIG. 1: Final variable distribution for the $H \to WW \to ee/\mu\mu$ analysis in the 0,1, and 2-jet sub-channels.

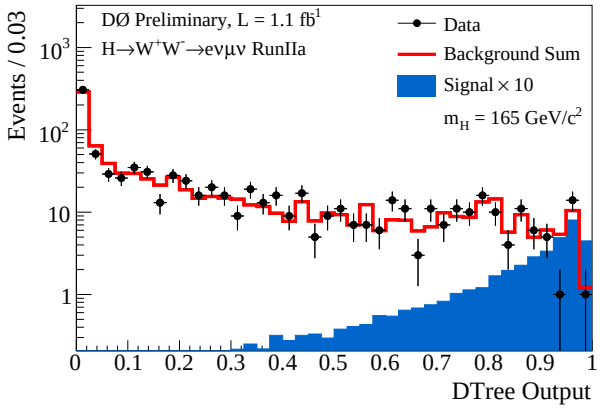

(a) $H \to WW \to e\mu$ Run IIa

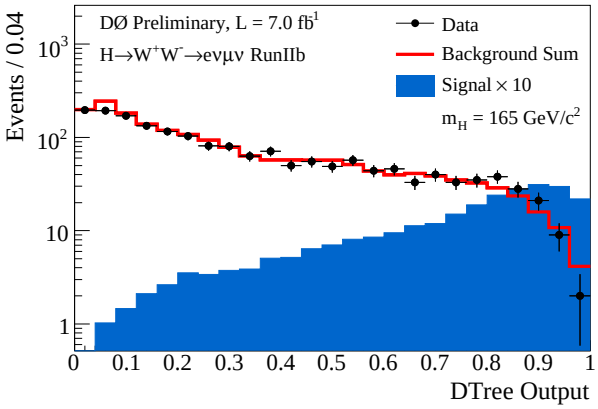

(b) $H \to WW \to ee\mu$ Run IIb

FIG. 2: Final variable distribution for the $H \to WW \to e\mu$ analysis in the Run IIa and Run IIb data epochs, both summing over the 0,1, and 2-jet sub-channels.

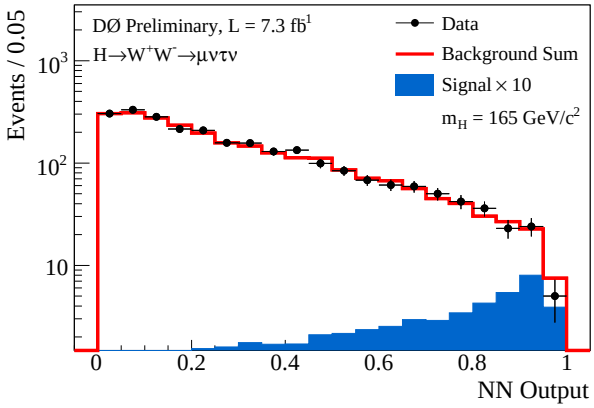

(a) $H \to WW \to \mu\tau$

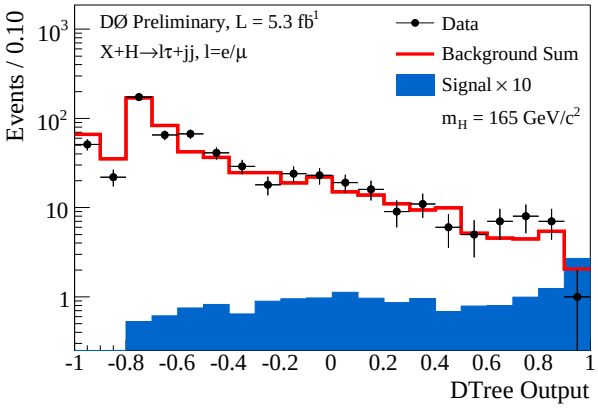

(b) $XS \to e/\mu\tau + jj$

FIG. 3: Final variable distribution for the $H \to WW \to \mu\tau$ analysis (left) and the $[XS \to e/\mu\tau + jj$ analysis (right).

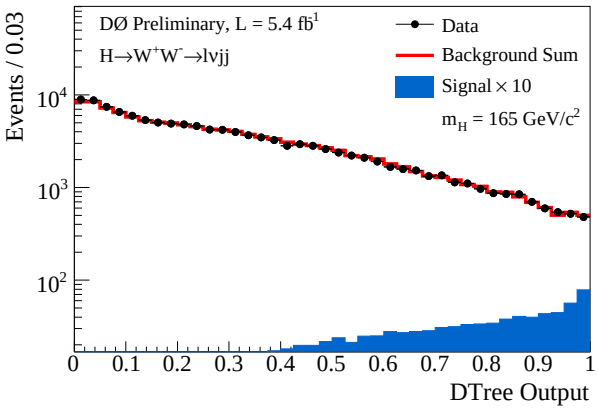

(a) $H \to W^+W^- \to \ell\nu q\bar{q}$

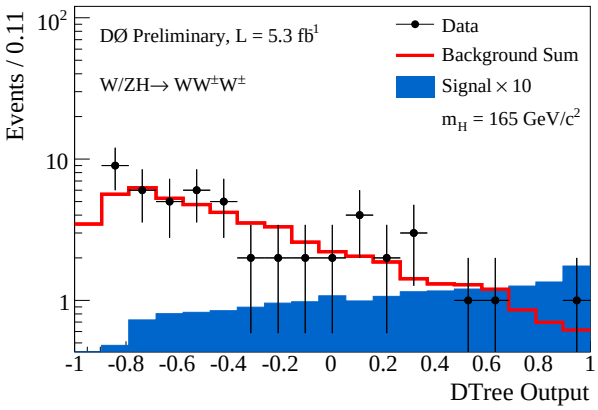

(b) $W/ZH \to WWW$

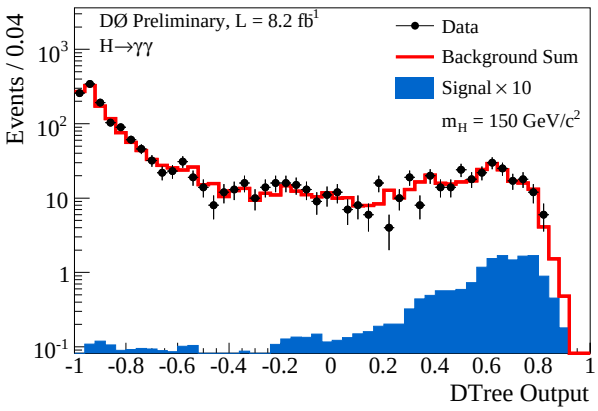

(c) $H \to \gamma\gamma$

FIG. 4: Final variable distribution for the $H \to W^+W^- \to \ell\nu q\bar{q}$ analysis combined over all lepton channels combined (top left), the $W/ZH \to WWW$ analysis combined over all lepton channels combined (top right) and the $H \to \gamma\gamma$ analysis (bottom).

TABLE III: Systematic uncertainties on the signal and background contributions for the $H \to W^+W^- \to \ell^\pm\ell^\mp$ channels. Systematic uncertainties are listed by name; see the original references for a detailed explanation of their meaning and on how they are derived. Shape uncertainties are labeled with the "s" designation. Systematic uncertainties shown in this table are obtained for the $m_H = 165$ GeV Higgs selection. Uncertainties are relative, in percent, and are symmetric unless otherwise indicated.

$H \to W^+W^- \to \ell^\pm\ell^\mp$ channels relative uncertainties (%)

Contribution	Diboson	$Z/\gamma^* \to \ell\ell$	$W + jet/\gamma$	$t\bar{t}$	Multijet	H
Luminosity/Normalization	6	6	6	6	30	6
Cross Section	7	5	6	10	–	7-33
PDF	2.5	2.5	2.5	2.5	–	8-30
EM Identification	2.5	2.5	2.5	2.5	–	2.5
Muon Identification	4	4	4	4	–	4
Vertex Confirmation (s)	2-6	1-7	1-6	1-8	–	1-8
Jet identification (s)	2-5	2-5	2-5	2-5	–	2-5
Jet Energy Scale (s)	2-3	1-4	1-8	1-4	–	1-10
Jet Energy Resolution(s)	1-4	1-4	1-12	1-3	–	1-12
B-tagging	10	10	10	5	–	10

TABLE IV: Systematic uncertainties on the signal and background contributions for the $H \to W^+W^- \to \mu\nu\tau_{had}\nu$ channel. Systematic uncertainties are listed by name; see the original references for a detailed explanation of their meaning and on how they are derived. Shape uncertainties are labeled with the shape designation (s). Systematic uncertainties shown in this table are obtained for the $m_H = 165$ GeV Higgs selection. Uncertainties are relative, in percent, and are symmetric unless otherwise indicated.

$H \to W^+W^- \to \mu\nu\tau_{had}\nu$ channel relative uncertainties (%)

Contribution	Diboson	$Z/\gamma^* \to \ell\ell$	$W +$ jets	$t\bar{t}$	Multijet	H
Luminosity ($\sigma_{\rm inel}(p\bar{p})$)	4.6	4.6	-	4.6	-	4.6
Luminosity Monitor	4.1	4.1	-	4.1	-	4.1
Trigger	5.0	5.0	-	5.0	-	5.0
Lepton ID	3.7	3.7	-	3.7	-	3.7
EM veto	5.0	-	-	5.0	-	5.0
Tau Energy Scale (s)	1.0	1.1	-	<1	-	<1
Jet Energy Scale (s)	8.0	<1	-	1.8	-	2.5
Jet identification (s)	<1	<1	-	7.5	-	5.0
Multijet (s)	–	-	-	-	20-50	-
Cross Section	7.0	4.0	-	10	-	10
Modeling	1.0	-	10	-	-	3.0

performed to both the background-only (b) and signal-plus-background (s+b) hypothesis separately for each Poisson MC trial.

IV. DERIVED UPPER LIMITS

We derive limits, at 95% C.L., on SM Higgs boson production $\sigma \times BR(H \to W^+W^-/\tau^+\tau^-/\gamma\gamma)$ via 34 individual channels [4–9]. To facilitate model transparency and to accommodate analyses with different degrees of sensitivity, we present our results in terms of the ratio of 95% C.L. upper cross section limits to the SM predicted cross section as a function of Higgs boson mass. The SM prediction for Higgs boson production would therefore be considered excluded at 95% C.L. when this limit ratio falls below unity.

The individual analyses described in Table I are grouped to evaluate combined limits over the range $130 \leq M_H \leq 200$ GeV. The $H \to \gamma\gamma$ analysis contributes to the region $M_H \leq 150$ GeV, while the rest of analyses contribute to the full mass range considered.

Figure 5 shows the expected and observed 95% C.L. cross section limit as a ratio to the SM cross sections and

TABLE V: Systematic uncertainties on the signal and background contributions for the $H \to WW^* \to lvjj$ electron and muon channels. Systematic uncertainties are listed by name; see the original references for a detailed explanation of their meaning and on how they are derived. Signal uncertainties are shown for $m_H = 160$ GeV for all channels except for WH, shown for $m_H = 115$ GeV. Those affecting the shape of the DTree discriminant are indicated with "Y." Uncertainties are listed as relative changes in normalization, in percent, except for those also marked by "S," where the overall normalization is constant, and the value given denotes the maximum percentage change from nominal in any region of the distribution.

$H \to WW^* \to lvjj$ Run II channel relative uncertainties (%)

Contribution	Shape	W+jets	Z+jets	Top	Diboson	$gg \to H$	$qq \to qqH$	WH
Jet energy scale	Y	$\binom{+6.7}{-5.4}^S$	< 0.1	± 0.7	± 3.3	$\binom{+5.7}{-4.0}$	± 1.5	$\binom{+2.7}{-2.3}$
Jet identification	Y	$\pm 6.6^S$	< 0.1	± 0.5	± 3.8	± 1.0	± 1.1	± 1.0
Jet resolution	Y	$\binom{+6.6}{-4.1}^S$	< 0.1	± 0.5	$\binom{+1.0}{-0.5}$	$\binom{+3.0}{-0.5}$	± 0.8	± 1.0
Association of jets with PV	Y	$\pm 3.2^S$	$\pm 1.3^S$	± 1.2	± 3.2	± 2.9	± 2.4	$\binom{+0.9}{-0.2}$
Luminosity	N	n/a	n/a	± 6.1	± 6.1	± 6.1	± 6.1	± 6.1
Muon trigger	Y	$\pm 0.4^S$	< 0.1	< 0.1	< 0.1	< 0.1	< 0.1	< 0.1
Electron identification	N	± 4.0	± 4.0	± 4.0	± 4.0	± 4.0	± 4.0	± 4.0
Muon identification	N	± 4.0	± 4.0	± 4.0	± 4.0	± 4.0	± 4.0	± 4.0
ALPGEN tuning	Y	$\pm 1.1^S$	$\pm 0.3^S$	n/a	n/a	n/a	n/a	n/a
Cross Section	N	± 6	± 6	± 10	± 7	± 10	± 10	± 6
Heavy-flavor fraction	Y	± 20	± 20	n/a	n/a	n/a	n/a	n/a
PDF	Y	$\pm 2.0^S$	$\pm 0.7^S$	$< 0.1^S$	$< 0.1^S$	$< 0.1^S$	$< 0.1^S$	$< 0.1^S$
			Electron channel			Muon channel		
Multijet Background	Y		± 6.5			± 26		

for the probed mass region ($130 \leq M_H \leq 200$ GeV), with all analyses combined. These results are also summarized in Table X. The LLR distributions for the full combination are shown in Fig. 6. Included in these figures are the median LLR values for the signal-plus-background hypothesis (LLR_{s+b}), background-only hypothesis (LLR_b), and the observed data (LLR_{obs}). The shaded bands represent the 1 and 2 standard deviation (σ) departures for LLR_b. These distributions can be interpreted as follows:

- The separation between LLR_b and LLR_{s+b} provides a measure of the discriminating power of the search. This is the ability of the analysis to separate the $s + b$ and $b-$only hypotheses.
- The width of the LLR_b distribution (shown here as one and two standard deviation (σ) bands) provides an estimate of how sensitive the analysis is to a signal-like background fluctuation in the data, taking account of the presence of systematic uncertainties. For example, when a 1σ background fluctuation is large compared to the signal expectation, the analysis sensitivity is thereby limited.
- The value of LLR_{obs} relative to LLR_{s+b} and LLR_b indicates whether the data distribution appears to be more like signal-plus-background or background-only. As noted above, the significance of any departures of LLR_{obs} from LLR_b can be evaluated by the width of the LLR_b distribution.

Figure 7 illustrates the exclusion criterion $1 - CL_s$ for the region $130 \leq m_H \leq 200$ GeV. In addition, we provide in Fig. 8 the values for the observed 1-CL_{s+b} and its expected distribution as a function of m_H. The value CL_{s+b} is the p-value for the signal+background hypothesis. These values can be used as an alternative to the CL_s method to obtain upper limits. The $CL_s = CL_{s+b}/CL_b$ formulation is intended to avoid setting limits when the background model grossly over-predicts the data or the data exhibits a large background-like fluctuation, as the value of CL_b will approach zero and the CL_s metric thus asymptotically limits the power of the search in such cases. When deriving limits via the p-value 1-CL_{s+b}, a power constraint can be introduced *a priori* to provide a similar protection against downward fluctuations in the data. For example, this can be done using a constraint that limits the exclusion metric at the -1σ background fluctuation level. This "power-constrained limit" method provides by construction stronger expected limits (comparing Figs. 7 and 8, the expected mass region excluded at the 95% C.L. grows by $\sim 40\%$), but also can lead to slightly larger false exclusion probabilities than the CL_s method and results in a less symmetric distribution of background fluctuations around the expected limit.

TABLE VI: Systematic uncertainties on the signal and background contributions for the $VH \to \ell^{\pm}\ell^{\pm} + X$ channels. Systematic uncertainties are listed by name; see the original references for a detailed explanation of their meaning and on how they are derived. Shape uncertainties are labeled with the "shape" designation. Systematic uncertainties for signal shown in this table are obtained for $m_H = 165$ GeV. Uncertainties are relative, in percent, and are symmetric unless otherwise indicated.

$VH \to \ell^{\pm}\ell^{\pm} + X$ Run IIa channel relative uncertainties (%)

Contribution	WZ/ZZ	W+jet	ChargeFlip	Multijet	$VH \to llX$
Cross section	7	6	0	0	0
Normalization	4	4	0	0	0
Trigger ($\mu\mu$)	0	0	0	0	2
LeptonID (ee)	8.6	8.6	0	0	8.6
LeptonID ($\mu\mu$)	4	4	0	0	4
LeptonID ($e\mu$)	6.3	6.3	0	0	6.3
JetID/JES	2	2	0	0	2
Jet-Lepton Fake	0	20	0	0	0
Instrumental (ee)	0	0	0	52	44
Instrumental ($e\mu$	0	0	0	0	29
Instrumental ($\mu\mu$)	0	0	0	155	42
Instrumental Model	-	-	shape	shape	-

$VH \to \ell^{\pm}\ell^{\pm} + X$ Run IIb channel relative uncertainties (%)

Contribution	WZ/ZZ	W+jet	ChargeFlip	Multijet	$VH \to llX$
Cross section	7	6	0	0	0
Normalization	4	4	0	0	0
Trigger ($\mu\mu$)	0	0	0	0	5
LeptonID (ee)	8.6	8.6	0	0	8.6
LeptonID ($\mu\mu$)	4	4	0	0	4
LeptonID ($e\mu$)	6.3	6.3	0	0	6.3
JetID/JES	2	2	0	0	2
Jet-Lepton Fake	0	20	0	0	0
Instrumental (ee)	0	0	0	23	31
Instrumental ($e\mu$)	0	0	0	0	19
Instrumental ($\mu\mu$)	0	0	0	43	28
Instrumental Model	-	-	shape	shape	-

V. CONCLUSIONS

We have presented upper limits on standard model Higgs boson production derived from 35 Higgs search analyses including data corresponding to 4.3-8.2fb^{-1} (See Table I). We have combined these analyses and form new limits more sensitive than each individual limit. The observed 95% C.L. upper limits are found to be a factor of 0.75 times the predicted standard model cross section at M_H =165 GeV while the expected limit is found to be a factor of 0.92 times the standard model prediction for the same mass. We exclude at the 95% C.L. the region $163 < M_H < 168$ GeV with an a-priori expected exclusion of $160 < M_H < 168$ GeV.

TABLE VII: Systematic uncertainties on the signal and background contributions for the $\tau\tau jj$ Run IIb channel. Systematic uncertainties for the Higgs signal shown in this table are obtained for $m_H = 135$ GeV. Systematic uncertainties are listed by name; see the original references for a detailed explanation of their meaning and on how they are derived. Uncertainties are relative, in percent, and are symmetric unless otherwise indicated. A systematic is denoted as flat if it affects the normalization only, and as 'shape' otherwise.

$\mu\tau_{had}jj$ Run IIb channel relative uncertainties (%)

Contribution	VH Signal	VBF Signal	GGF Signal	$W + jets$	$Z + jets$	Top	diboson	Multijet
Luminosity (D0 specific)	4.1	4.1	4.1	4.1	4.1	4.1	4.1	-
Luminosity (Tevatron common)	4.6	4.6	4.6	4.6	4.6	4.6	4.6	-
μ ID	2.9	2.9	2.9	2.9	2.9	2.9	2.9	-
μ trigger	8.6	8.6	8.6	8.6	8.6	8.6	8.6	-
τ energy correction	9.8	9.8	9.8	9.8	9.8	9.8	9.8	-
τ track efficiency	1.4	1.4	1.4	1.4	1.4	1.4	1.4	-
τ selection by type	12,4.2,7	12,4.2,7	12,4.2,7	12,4.2,7	12,4.2,7	12,4.2,7	12,4.2,7	-
Cross section	6.2	4.9	33	6.0	6.0	10.0	7.0	-
GGF Signal PDF	-	-	29	-	-	-	-	-
GGF Hp_T Reweighting (Shape)	1.0	1.0	1.0	1.0	1.0	1.0	1.0	-
Vertex confirmation for jets	4.0	4.0	4.0	4.0	4.0	4.0	4.0	-
Jet ID(Shape)	$\sim$10	$\sim$10	$\sim$10	$\sim$10	$\sim$10	$\sim$10	$\sim$10	-
Jet Energy Resolution (Shape)	$\sim$10	$\sim$10	$\sim$10	$\sim$10	$\sim$10	$\sim$10	$\sim$10	-
Jet energy Scale (Shape)	$\sim$15	$\sim$15	$\sim$15	$\sim$15	$\sim$15	$\sim$15	$\sim$15	-
Jet pT	5.5	5.5	5.5	5.5	5.5	5.5	5.5	-
PDF reweighting	2	2	2	2	2	2	2	-
Multijet Normalization	-	-	-	-	-	-	-	5.3
Multijet Shape	-	-	-	-	-	-	-	$\sim$15

$e\tau_{had}jj$ Run IIb relative uncertainties (%)

Contribution	VH Signal	VBF Signal	GGF Signal	$W + jets$	$Z + jets$	Top	diboson	Multijet
Luminosity (D0 specific)	4.1	4.1	4.1	4.1	4.1	4.1	4.1	-
Luminosity (Tevatron common)	4.6	4.6	4.6	4.6	4.6	4.6	4.6	-
EM ID	4	4	4	4	4	4	4	-
e trigger	2	2	2	2	2	2	2	-
τ energy correction	9.8	9.8	9.8	9.8	9.8	9.8	9.8	-
τ track efficiency	1.4	1.4	1.4	1.4	1.4	1.4	1.4	-
τ selection by type	12,4.2,7	12,4.2,7	12,4.2,7	12,4.2,7	12,4.2,7	12,4.2,7	12,4.2,7	-
Cross section	6.2	4.9	33	6.0	6.0	10.0	7.0	-
GGF Signal PDF	-	-	29	-	-	-	-	-
GGF Hp_T Reweighting (Shape)	1.0	1.0	1.0	1.0	1.0	1.0	1.0	-
Vertex confirmation for jets	4.0	4.0	4.0	4.0	4.0	4.0	4.0	-
Jet ID(Shape)	$\sim$10	$\sim$10	$\sim$10	$\sim$10	$\sim$10	$\sim$10	$\sim$10	-
Jet Energy Resolution (Shape)	$\sim$10	$\sim$10	$\sim$10	$\sim$10	$\sim$10	$\sim$10	$\sim$10	-
Jet energy Scale (Shape)	$\sim$15	$\sim$15	$\sim$15	$\sim$15	$\sim$15	$\sim$15	$\sim$15	-
Jet pT	5.5	5.5	5.5	5.5	5.5	5.5	5.5	-
PDF reweighting	2	2	2	2	2	2	2	-
Multijet Normalization	-	-	-	-	-	-	-	4.7
Multijet Shape	-	-	-	-	-	-	-	$\sim$15

Acknowledgments

We thank the staffs at Fermilab and collaborating institutions, and acknowledge support from the DOE and NSF (USA); CEA and CNRS/IN2P3 (France); FASI, Rosatom and RFBR (Russia); CNPq, FAPERJ, FAPESP and FUNDUNESP (Brazil); DAE and DST (India); Colciencias (Colombia); CONACyT (Mexico); KRF and KOSEF (Korea); CONICET and UBACyT (Argentina); FOM (The Netherlands); STFC and the Royal Society (United Kingdom); MSMT and GACR (Czech Republic); CRC Program and NSERC (Canada); BMBF and DFG (Germany);

TABLE VIII: Systematic uncertainties on the signal and background contributions for the $H \to \gamma\gamma$ channel. Systematic uncertainties for the Higgs signal shown in this table are obtained for $m_H = 125$ GeV. Systematic uncertainties are listed by name; see the original references for a detailed explanation of their meaning and on how they are derived. Uncertainties are relative, in percent, and are symmetric unless otherwise indicated.

$H \to \gamma\gamma$ channel relative uncertainties (%)

Contribution	Background	Signal
Luminosity	6	6
Acceptance	–	2
electron ID efficiency	2	–
electron track-match inefficiency	10	–
Photon ID efficiency	3	3
Photon energy scale	2	1
Cross Section	4	10
Background subtraction	15	-

SFI (Ireland); The Swedish Research Council (Sweden); and CAS and CNSF (China).

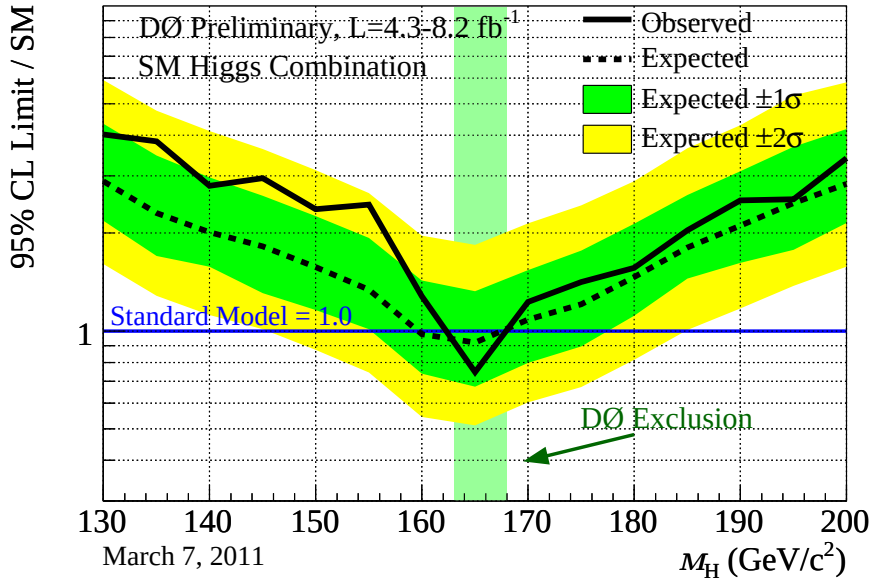

FIG. 5: Expected (median) and observed 95% C.L. cross section upper limit ratios for the combined $WH/ZH/H, H \to W^+W^-/\gamma\gamma/\tau^+\tau^-$ analyses over the $130 \leq M_H \leq 200$ GeV mass range.

TABLE IX: The correlation matrix for the analysis channels. All uncertainties within a group are considered 100% correlated across channels. The correlated systematic uncertainty on the background cross section (σ) is itself subdivided according to the different background processes in each analysis.

Source	$H\to W^+W^-\to\ell^\pm\nu\ell^\mp\nu$	$H+X\to\mu^\pm\tau^\mp_{had}+\leq 1j$	$H+X\to\ell^\pm\tau^\mp_{had}jj$	$H\to W^+W^-\to\ell\nu jj$
Luminosity	×	×	×	×
Normalization				
Jet Energy Scale	×	×	×	×
Jet ID	×	×	×	×
Tau Energy Scale/ID		×	×	
Electron ID/Trigger	×	×	×	×
Muon ID/Trigger	×	×	×	×
Photon ID/Trigger				
b-Jet Tagging				
Background σ	×	×	×	×
Background Modeling				
Multijet				
Signal σ	×	×	×	×
Signal modeling	×	×	×	×

Source	$VH\to\ell^\pm\ell^\pm+X$	$H\to\gamma\gamma$
Luminosity		×
Normalization		
Jet Energy Scale	×	
Jet ID	×	
Tau Energy Scale/ID		
Electron ID/Trigger	×	
Muon ID/Trigger	×	
Photon ID/Trigger		×
b-Jet Tagging		
Background σ	×	
Background Modeling		
Multijet		
Signal σ	×	×
Signal modeling	×	×

TABLE X: Combined 95% C.L. limits on $\sigma\times BR(H\to W^+W^-/\gamma\gamma/\tau^+\tau^-)$ for SM Higgs boson production. The limits are reported in units of the SM production cross section times branching fraction.

M_H (GeV)	130	135	140	145	150	155	160	165	170	175	180	185	190	195	200
Expected:	2.88	2.31	2.01	1.82	1.57	1.34	0.98	0.92	1.08	1.21	1.47	1.81	2.11	2.47	2.83
Observed:	4.02	3.84	2.80	2.95	2.37	2.45	1.28	0.75	1.23	1.41	1.56	2.04	2.52	2.54	3.40

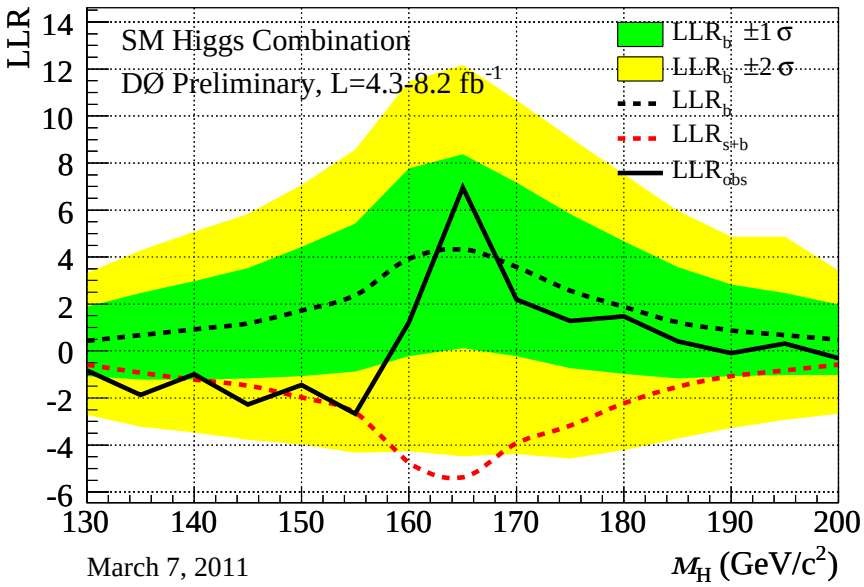

FIG. 6: Log-likelihood ratio distribution for the combined $WH/ZH/H, H \to W^+W^-/\gamma\gamma/\tau^+\tau^-$ analyses over the $130 \leq M_H \leq 200$ GeV mass range.

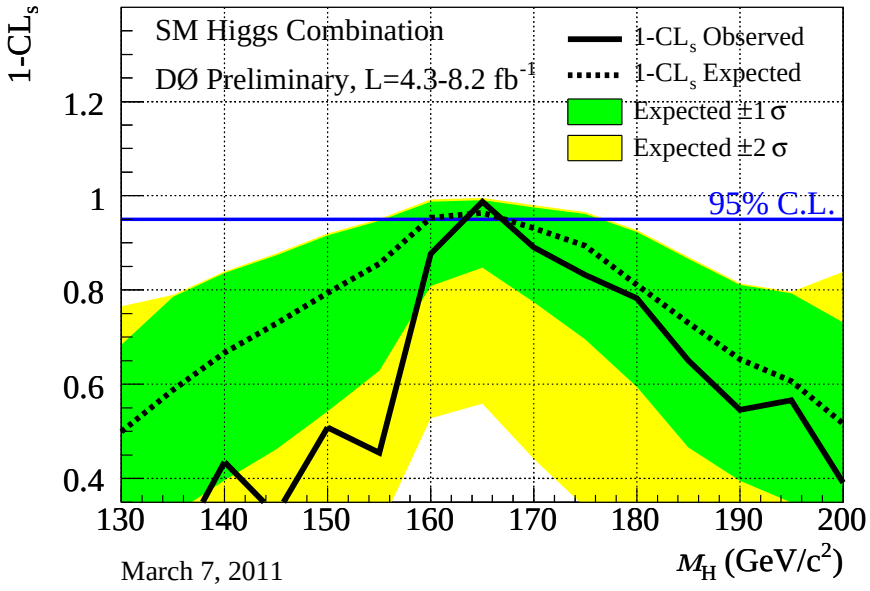

FIG. 7: The $1 - CL_S$ (exclusion probability) distribution for the combined $WH/ZH/H, H \to W^+W^-/\gamma\gamma/\tau^+\tau^-$ analyses over the $130 \leq M_H \leq 200$ GeV mass range.

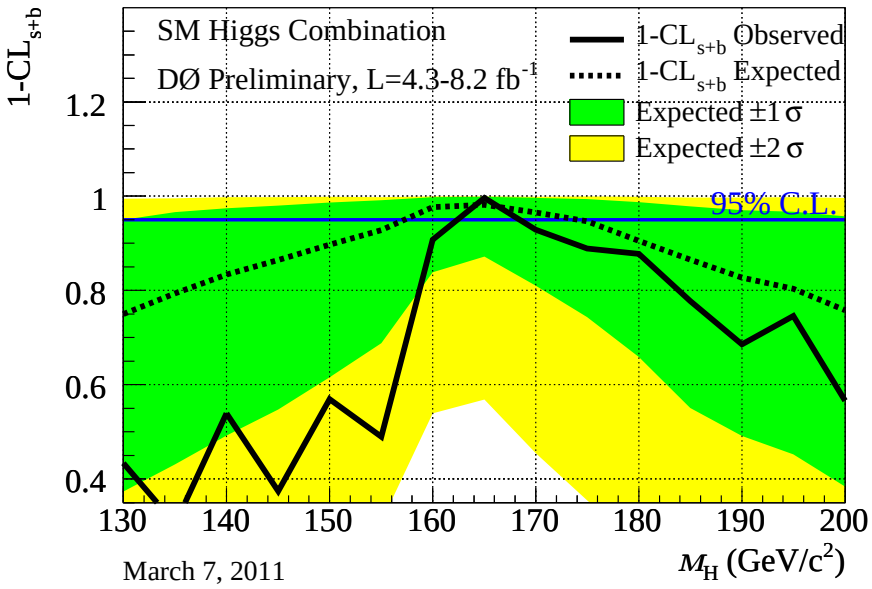

FIG. 8: The $1-CL_{S+b}$ (signal+background p-value) distribution for the combined $WH/ZH/H, H\to W^+W^-/\gamma\gamma/\tau^+\tau^-$ analyses over the $130 \leq M_H \leq 200$ GeV mass range.

[1] R. Barate *et al.* [LEP Working Group for Higgs boson searches], Phys. Lett. B **565**, 61 (2003), [arXiv:hep-ex/0306033].
[2] The LEP Electroweak Working Group, "Status of July 2010", http://lepewwg.web.cern.ch/LEPEWWG/.
[3] DØ Collaboration, V. Abazov *et. al.*, Nucl. Instrum. Meth. A **565**, 463 (2006) [arXiv:hep-ph/0507191].
[4] DØ Collaboration, DØ Note 6182-CONF.
[5] DØ Collaboration, e-Print: arXiv:1101.6079v2 [hep-ph].
[6] DØ Collaboration, DØ Note 6179-CONF.
[7] DØ Collaboration, DØ Note 6171-CONF.
[8] DØ Collaboration, DØ Note 6091-CONF.
[9] DØ Collaboration, DØ Note 5858-CONF.
[10] DØ Collaboration, DØ Note 6094-CONF.
[11] T. Sjöstrand, L. Lonnblad and S. Mrenna, "PYTHIA 6.2: Physics and manual," arXiv:hep-ph/0108264.
[12] M. L. Mangano, M. Moretti, F. Piccinini, R. Pittau and A. D. Polosa, "ALPGEN, a generator for hard multiparton processes in hadronic collisions," JHEP **0307**, 001 (2003).
[13] A. Pukhov *et al.*, "CompHEP: A package for evaluation of Feynman diagrams and integration over multi-particle phase space. User's manual for version 33," [arXiv:hep-ph/9908288].
[14] J. Campbell and R. K. Ellis, http://mcfm.fnal.gov/.
J. M. Campbell, R. K. Ellis, Nucl. Phys. Proc. Suppl. **205-206**, 10-15 (2010). [arXiv:1007.3492 [hep-ph]].
[15] The CDF and DZ Collaborations and the TEVNPHWG Working Group, "Combined CDF and DZ Upper Limits on Standard Model Higgs-Boson Production with up to 8.2 fb^{-1} of Data", FERMILAB-CONF-11-044-E, CDF Note 10441, DZ Note 6184.
[16] C. Anastasiou, R. Boughezal and F. Petriello, JHEP **0904**, 003 (2009).
[17] D. de Florian and M. Grazzini, Phys. Lett. B **674**, 291 (2009).
[18] M. Grazzini, private communication (2010).
[19] The CDF and DZ Collaborations and the Tevatron Electroweak Working Group, arXiv:1007.3178 [hep-ex], arXiv:0903.2503 [hep-ex].
[20] R. V. Harlander and W. B. Kilgore, Phys. Rev. Lett. **88**, 201801 (2002).
[21] C. Anastasiou and K. Melnikov, Nucl. Phys. B **646**, 220 (2002).
[22] V. Ravindran, J. Smith, and W. L. van Neerven, Nucl. Phys. B **665**, 325 (2003).
[23] S. Actis, G. Passarino, C. Sturm, and S. Uccirati, Phys. Lett. B **670**, 12 (2008).
[24] U. Aglietti, R. Bonciani, G. Degrassi, A. Vicini, "Two-loop electroweak corrections to Higgs production in proton-proton collisions", arXiv:hep-ph/0610033v1 (2006).
[25] S. Catani, D. de Florian, M. Grazzini and P. Nason, "Soft-gluon resummation for Higgs boson production at hadron colliders," JHEP **0307**, 028 (2003) [arXiv:hep-ph/0306211].
[26] A. D. Martin, W. J. Stirling, R. S. Thorne and G. Watt, Eur. Phys. J. C **63**, 189 (2009).
[27] `http://www.hep.ucl.ac.uk/pdf4lhc/`;
S. Alekhin *et al.*, (PDF4LHC Working Group), [arXiv:1101.0536v1 [hep-ph]];
M. Botje *et al.*, (PDF4LHC Working Group), [arXiv:1101.0538v1 [hep-ph]].
[28] P. M. Nadolsky *et al.*, Phys. Rev. D **78**, 013004 (2008) [arXiv:0802.0007 [hep-ph]].
[29] R. D. Ball *et al.* [NNPDF Collaboration], Nucl. Phys. B **809**, 1 (2009) [Erratum-ibid. B **816**, 293 (2009)] [arXiv:0808.1231 [hep-ph]].
[30] C. Anastasiou, G. Dissertori, M. Grazzini, F. Stöckli and B. R. Webber, JHEP **0908**, 099 (2009).
arXiv:1102.3182 [hep-ph] (2011).
[31] J. M. Campbell, R. K. Ellis, C. Williams, Phys. Rev. **D81**, 074023 (2010). [arXiv:1001.4495 [hep-ph]].
[32] H. L. Lai *et al.*, Phys. Rev D **55**, 1280 (1997).
[33] G. Bozzi, S. Catani, D. de Florian, and M. Grazzini, Phys. Lett. B **564**, 65 (2003); // G. Bozzi, S. Catani, D. de Florian, and M. Grazzini, Nucl. Phys. B **737**, 73 (2006).
[34] C. Balazs, J. Huston, I. Puljak, Phys. Rev. D **63** 014021 (2001).
C. Balazs and C.-P. Yuan, Phys. Lett. B **478** 192-198 (2000).
Qing-Hong Cao and Chuan-Ren Chen, Phys. Rev. D **76** 073006 (2007).

[35] C. Anastasiou, private communication (2010).
[36] J. Baglio and A. Djouadi, JHEP **1010**, 064 (2010) [arXiv:1003.4266v2 [hep-ph]].
[37] The Fortran program can be found on Michael Spira's web page `http://people.web.psi.ch/~mspira/proglist.html`.
[38] O. Brein, A. Djouadi, and R. Harlander, Phys. Lett. B **579**, 149 (2004).
[39] M. L. Ciccolini, S. Dittmaier, and M. Kramer, Phys. Rev. D **68**, 073003 (2003).
[40] P. Bolzoni, F. Maltoni, S.-O. Moch, and M. Zaro, Phys. Rev. Lett. **105**, 011801 (2010) [arXiv:1003.4451v2 [hep-ph]].
[41] M. Ciccolini, A. Denner, and S. Dittmaier, Phys. Rev. Lett. **99**, 161803 (2007) [arXiv:0707.0381 [hep-ph]];
M. Ciccolini, A. Denner, and S. Dittmaier, Phys. Rev. D **77**, 013002 (2008) [arXiv:0710.4749 [hep-ph]].
We would like to thank the authors of the HAWK program for adapting it to the Tevatron.
[42] A. Djouadi, J. Kalinowski and M. Spira, Comput. Phys. Commun. **108**, 56 (1998).
[43] J. Baglio and A. Djouadi, arXiv:1012.0530 [hep-ph] (2010).

[44] T. Junk, Nucl. Intrum. Meth. A **434**, 435 (1999); A.Read, CERN 2000-005 (30 May 2000).
[45] T. Andeen *et al.*, Report No. FERMILAB-TM-2365, 2007.
[46] W. Fisher, FERMILAB-TM-2386-E.